Morphological Segmentation of Retinal Blood Vessels and Consequent Tortuosity Extraction

J. Kubicek[1], J. Timkovic[2], A. Krestanova[1], M. Augustynek[1], M. Penhaker[1] and I. Bryjova[1]
[1]*VSB–Technical University of Ostrava, FEECS, K450, 17. Listopadu 15, 708 33, Ostrava–Poruba, Czech Republic.*
[2]*Clinic of Ophthalmology, University Hospital Ostrava, Czech Republic.*
jan.kubicek@vsb.cz

***Abstract*—Investigation of a retinal blood vessel system is frequently discussed issue in the field of the clinical ophthalmology due to it serves as reliable indicator of retinal damage. The analysis deals with two coherent tasks regarding retinal blood vessels system. Firstly, the algorithm based on the morphological operations is proposed to be able to perform precise extraction and localization of individual blood vessels for further processing. On the base of this segmentation procedure, e obtain a segmentation model differentiating the retinal blood vessels from retinal background. The second step deals with the major output of the analysis it is tortuosity extraction as it is parameter describing curvature of blood vessels. The tortuosity allows for a description of each vessel element by level of a curvature. It is significantly beneficial for clinical practice, because on the base of blood vessel curvature, physiological or damaged retinal system can be recognized.**

***Index Terms*—Retinal Blood Vessels; Image Segmentation; Tortuosity; Mathematical Morphology.**

I. Introduction

Analysis of retinal blood vessels is closely related to the retinopathy of prematurity (ROP). ROP was originally designated as retrolental fibroplasias by Terry in 1952 who related it with premature birth. Term ROP was coined by Heath in 1951. It is a disorder of development of retinal blood vessels in premature babies. Normal retinal vascularization happens centrifugally from optic disc to ora. Vascularization up to nasal ora is completed by 8 months (36 weeks) and temporal ora by 10 months (39–41 weeks). During ROP development, retinal changes on eye background are classified from the view of their localization and scale of change. The ROP screening target is an early detection, and treatment timing of thresholded or pre-thresholded ROP stages. All children born before 31 gestational, or birthweight fewer than 1500 g have to undergo the ROP screening treatment. These children undergo the control examination after 1 to 2 weeks up to full vascularization of three zone. Children suffering for ROP must be, at the beginning of treatment, frequently medical checked, because it is necessary precise and early treatment. A reverse diagnosis can often cause complete blindness [1-6].

II. Clinical Specification of Tortuosity

Tortuosity (blood vessel curvature) is observed as blood vessel anomaly affecting of different types of blood streams. They can be blood streams through nearly all body parts including large arteries and veins, but also smaller arteries and tiny veins. Slightly curved or twisted blood vessels without clinical signs are common deviation observed on people and animals. Nevertheless, a severe tortuosity can lead to different severe symptoms [8-11].

Blood vessel curving is clinically related with ageing, atherosclerosis, hypertension, genetic defects and diabetes mellitus. Nevertheless, the mechanisms causing blood vessel curving are not sufficiently investigated yet. Blood vessels are commonly direct, in order to be possible supply of organs by blood. Blood vessel anomalies can be observed by medical imagining systems for instance RetCam 3. Figure 2 depicts of individual tortuosity forms of blood vessels [12-15].

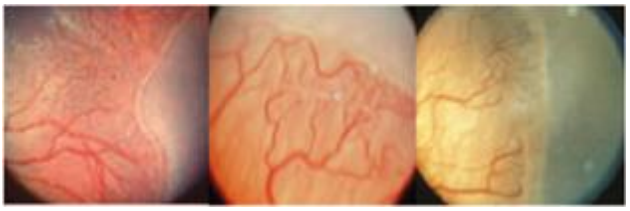

(a) (b) (c)

Figure 1: Individual stages of ROP, (a) 1. Stage, (b) 2. Stage, (c) 3. Stage [7]

(a) (b) (c) (d)

Figure 2: Different tortuosity forms, (a) curving, (b) breaking, (c) knot, and (d) torsion [13]

III. Design of Algorithm for Retinal Vessels Segmentation

The first part of the proposed solution is algorithm serving for automatic extraction of blood vessels from retinal images. The major problem we faced with is quality and contrast of retinal records. Retinal images from system RetCam 3 are generated in 480x640 pixels. In the dependence of lower resolution, the images have worse contrast leading to the fact that blood vessels are badly recognizable. On the base this unfavorable phenomenon, the proposed algorithm must be sensitive even in the noisy environment and sufficiently robust. Therefore, we propose algorithm including comprehensive image preprocessing procedure serving for adjusting of input images for further processing. After it, morphological segmentation process is applied. The overall segmentation structure is depicted on Figure 3.

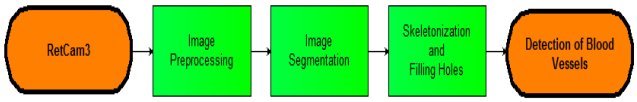

Figure 3: Algorithm design for retinal blood vessel system segmentation

A. *Image Preprocessing*

As it was aforementioned, image preprocessing serves for better blood vessels observation, to be achieved as precise blood vessel detection as possible. The overall image preprocessing structure is depicted on Figure 4.

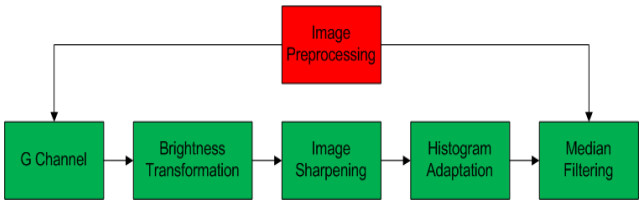

Figure 4: Flow chart of retinal image preprocessing procedure

It is supposed that retinal image is acquired in RGB format. On the experimental basis it is found that blood vessel system is the best observable from G layer, therefore we use this layer with gray level conversion for further processing (Figure 5).

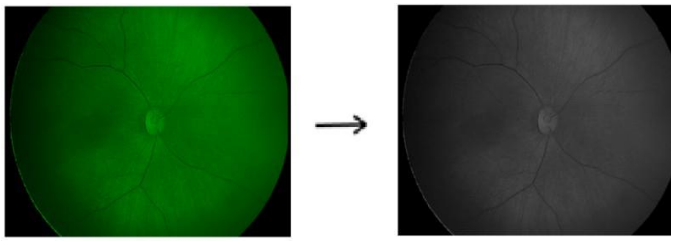

Figure 5: G layer transformation to gray scale level (monochromatic image format)

Consequently it is applied combination image sharpening with histogram adaptation for achieving better differentiation between blood vessels and retinal background. The comparison between sharpening procedure and histogram adaption is depicted on Figure 6.

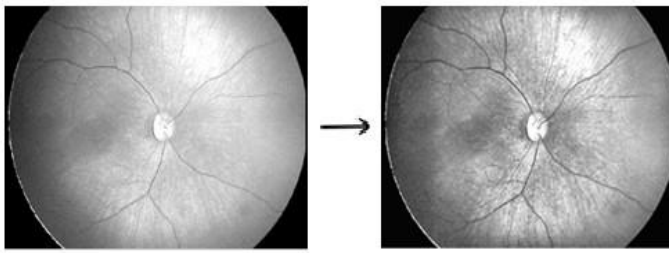

Figure 6: Image sharpening (left), histogram adaptation (right)

The concluding image preprocessing step deals with median filtration. It is supposed that retinal records are slightly corrupted by noise, especially, caused by lower scanning resolution. For the mentioned reason, median filtration is applied for image smoothing, and adjusting the resulting image.

B. *Morphological Image Segmentation*

The segmentation procedure (Figure 7) is based on the consequential morphological approach including morphological dilation, close procedure, and Canny operator. The edge detection seeks for edges on the base of zero crossing of second order derivative. In the first step, the image gradient is approximated in the x axis direction (K_{GX}) and y direction (K_{GY}).

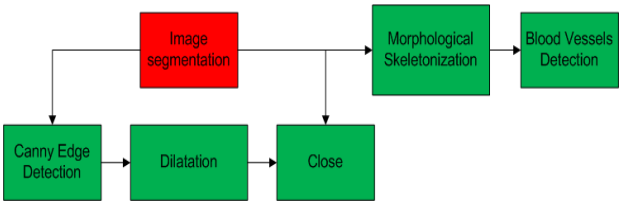

Figure 7: Overall structure of image segmentation

$$K_{GX} = \begin{bmatrix} -1 & 0 & 1 \\ -2 & 0 & 2 \\ -1 & 0 & 1 \end{bmatrix}, K_{GY} = \begin{bmatrix} 1 & 2 & 1 \\ 0 & 0 & 0 \\ -1 & -2 & -1 \end{bmatrix} \quad (1)$$

The edge strength (Equation (2)) is given by Euclidean distance between x gradient (G_x) and y gradient (G_y) from Equation (1) [1].

$$|G| = \sqrt{G_x^2 + G_Y^2} = |G_x| + |G_Y| \quad (2)$$

Consequently, morphological dilatation is applied. Dilatation sums of two sets with using of Minkowski sum. In the result of this operation, it goes to expanding objects in image and also to filling of holes. The dilatation is defined by the following Equation (3).

$$X \oplus B = \{p \in \varepsilon^2, p = x + b, x \in X, b \in B\} \quad (3)$$

Where $X \oplus B$ represents the point set of all existed vector sums for couple of pixels, one of them belonging to retinal image (X), second represents a morphological structural element (B). Parameter p denotes dilatation procedure and ε^2 image area. For practical purposes of segmentation, the line structural element is used. By using of the morphological close it is achieved dilatation with consequent erosion by same structural element. By this way, contour smoothing is achieved, connecting of tiny holes and also removing of small holes. Closing (4) is similar in some ways to dilation in that it tends to enlarge the boundaries of foreground (bright) regions in an image (and shrink background color holes in such regions), but it is less destructive of the original boundary shape. The morphological operation closing is defined by the following expression:

$$X \bullet B = (X \oplus B) \ominus B \quad (4)$$

The final part forming the resulting model of blood vessels is binary skeleton. The main aim of this operation is smoothing and simplifying of blood vessel structure. Output is a typological skeleton precisely describing shape of retinal blood vessel system. This process is given by the following Equation (5).

$$X \oplus B = X \backslash (X \otimes B) \quad (5)$$

The process is terminated when two subsequent steps have same result.

$$X \oplus \{B_i\} = (\left(\left(X \oplus B_{(1)}\right) \oplus B_{(2)}\right) \ldots \oplus B_n) \quad (6)$$

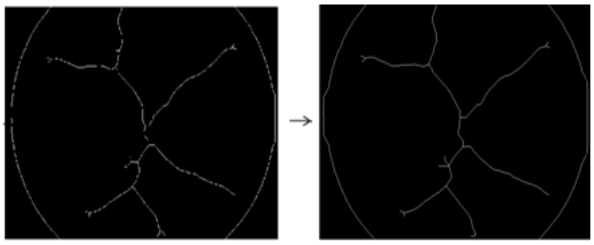

Figure 8: Algorithm testing for testing native data and mathematical model of respective blood vessels

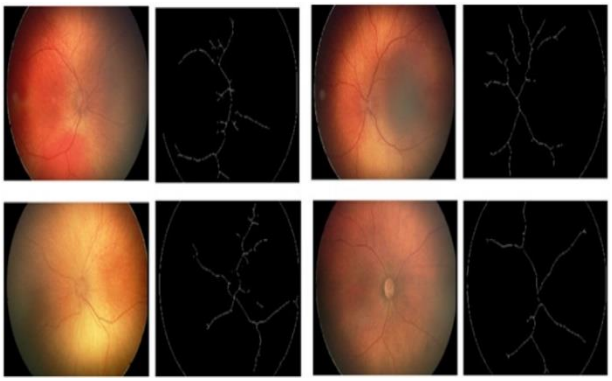

Figure 9: Algorithm testing for testing native data and mathematical model of respective blood vessels

Figure 9 shows algorithm outputs for real native data acquired from Ophthalmologic clinic University hospital in Ostrava. Within the testing phase, sample of 150 image records acquired by system RetCam 3 was analyzed. Mathematical model of retinal vessels system reliably approximates vessel morphological structure serves for extraction of tortuosity as curvature indicator.

IV. Extraction of Blood Vessels Tortuosity

It is supposed that curve (blood vessel) is parametrized by *s*:

$$C(s) = \begin{pmatrix} x(s) \\ y(s) \end{pmatrix} \quad (7)$$

Tangent is expressed by:

$$T(s) = \frac{1}{L}\begin{pmatrix} \dot{x}(s) \\ \dot{y}(s) \end{pmatrix} \quad (8)$$

where $L = \sqrt{\dot{x}(s)^2 + \dot{y}(s)^2}$, and normal is expressed by:

$$N(s) = \frac{1}{L}\begin{pmatrix} -\dot{y}(s) \\ \dot{x}(s) \end{pmatrix} \quad (9)$$

By definition *T.N=0*. The curvature radius is described by distance to the point of intersection of the two lines:

$$\begin{pmatrix} x(s_1) \\ y(s_1) \end{pmatrix} + \lambda N_1, \begin{pmatrix} x(s_2) \\ y(s_2) \end{pmatrix} + \lambda N_2 \quad (10)$$

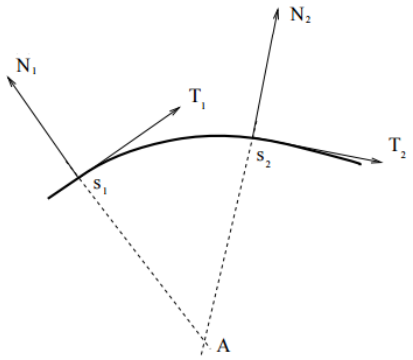

Figure 10: Relationship of tangent and normal vector in curvature

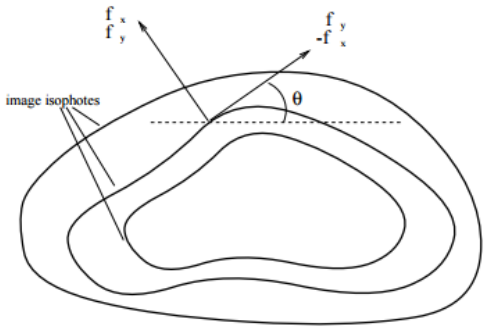

Figure 11: Image gradient is the normal to the lines of equal intensity (isophotes)

Finally we equate the contour normal to the image gradient (Figure 11).

$$N(x,y) = \frac{1}{\sqrt{f_x^2 + f_y^2}}\begin{pmatrix} f_x \\ f_y \end{pmatrix} \quad (11)$$

In comparison with Equation (9) means:

$$\dot{x}(s) = f_y, \dot{y}(s) = -f_x \quad (12)$$

The equality can be taken by imposing an appropriate parametrization. We need to define it by Equation (13).

$$\frac{d}{ds} = \frac{dx}{ds}\frac{d}{dx} + \frac{dy}{ds}\frac{d}{dy} = cos\theta\frac{d}{dx} + sin\theta\frac{d}{dy} \quad (13)$$

where:

$$cos\theta = \frac{\dot{x}(s)}{\sqrt{\dot{x}(s)^2 + \dot{y}(s)^2}} = \frac{f_y}{\sqrt{f_x^2 + f_y^2}}$$

$$sin\theta = \frac{\dot{y}(s)}{\sqrt{\dot{x}(s)^2 + \dot{y}(s)^2}} = \frac{-f_x}{\sqrt{f_x^2 + f_y^2}}$$

which leads to:

$$\ddot{x}(s) = cos\theta f_{yx} + sin\theta f_{yy} = \frac{f_y f_{yx}}{\sqrt{f_x^2+f_y^2}} + \frac{-f_x f_{yy}}{\sqrt{f_x^2+f_y^2}}$$

$$\ddot{y}(s) = -cos\theta f_{xx} - sin\theta f_{xy} = -\frac{f_y f_{xx}}{\sqrt{f_x^2+f_y^2}} - \frac{-f_x f_{xy}}{\sqrt{f_x^2+f_y^2}}$$

General form of curvature is given by Equation (14):

$$k(s) = \frac{\dot{T}(s).N(s)}{L^3} = -\frac{T(s).\dot{N}(s)}{L^3} = \frac{\dot{x}(s)\ddot{y}(s) - \dot{y}(s)\ddot{x}(s)}{(\dot{x}(s)^2 + \dot{y}(s)^2)^{3/2}} \quad (14)$$

On the base of Equation (14) we obtain final form of curvature by Equation (15) [16-18].

$$k(x,y) = -\frac{f_{xx}{f_y}^2 + f_{yy}{f_x}^2 - 2f_{xy}f_xf_y}{\left({f_x}^2 + {f_y}^2\right)^{3/2}} \quad (15)$$

As it was aforementioned, the tortuosity is parameter corresponding with blood vessels curvature. The major problem is that the tortuosity is not strictly defined. By definition tortuosity determines curvature of blood vessels. Algorithm allows for differentiation of individual blood vessels according to their curvature calculated in degrees. By this way we propose objective measurement of tortuosity allowing for blood vessel system segmentation in the context of color map where over thresholded blood vessel spots are marked by red (Figure 12). The comparison of thresholded values (20°, 50° and 120°) is depicted on Figure 13.

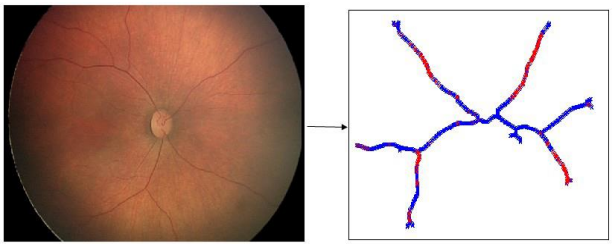

Figure 12: Native image (left), curvature estimation (right)

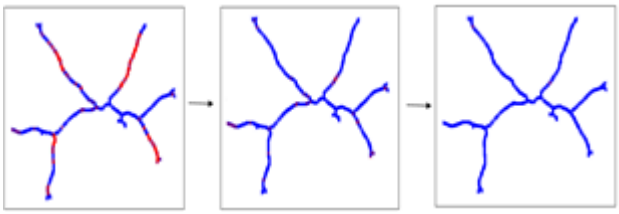

(a) (b) (c)

Figure 13: Comparison of set threshold, (a) threshold=20°, (b) threshold=50° and (c) threshold=120°

V. Conclusion

We propose a method for the automatic analysis of retinal blood vessel structures. Algorithm is composed from two essential parts. The Segmentation algorithm based on set of morphological operations serves for detection and consequent extraction of blood vessels. In the result we obtain the binary segmentation map where individual retinal blood vessels are represented by lines, other retinal structures are suppressed. This mathematical model is intended for extraction of blood vessels curvature. Second part of algorithm is intended for retinal blood vessels curvature estimation in every blood vessel element. Nevertheless, second important issue is clinical evaluation of tortuosity. Physicians are able to roughly estimate curvature from native images by naked eye, but they are not able to state of an accurate range of angles corresponding with tortuosity. In our future research we are going to devote to developing of expert system which will be able to estimate certain range of angles which would be, from clinical point of view representative for tortuosity assessment

Acknowledgment

The work and the contributions were supported by the project SV4506631/2101 'Biomedicínské inženýrské systémy XII'.

References

[1] S.S. Kar, S.P. Maity, Retinal blood vessel extraction and optic disc removal using curvelet transform and morphological operation (2015) *Advances in Intelligent Systems and Computing*, 390, pp. 153-161.

[2] D. Relan, L. Ballerini, E. Trucco, T. MacGillivray, Retinal vessel classification based on maximization of squared-loss mutual information (2016) *Advances in Intelligent Systems and Computing*, 390, pp. 77-84.

[3] A. Sodi, D.P. Mucciolo, V. Murro, C. Zoppetti, B. Terzuoli, A. Mecocci, G. Virgili, S. Rizzo, Computer-assisted evaluation of retinal vessel diameter in retinitis pigmentosa (2016) *Ophthalmic Research*, 56 (3), pp. 139-144.

[4] S. Sil Kar, S.P. Maity, Retinal blood vessel extraction using tunable bandpass filter and fuzzy conditional entropy (2016) *Computer Methods and Programs in Biomedicine*, 133, pp. 111-132.

[5] Z. Rezaei, A. Selamat, M. S. M. Rahim, and M. R. A. Kadir, Image segmentation of coronary artery plaque using intuitionistic fuzzy C-means algorithm, *Proceedings of International Conference on Artificial Life and Robotics (Icarob 2014)*, pp. 26-31, 2014.

[6] L. Sulik, O. Krejcar, A. Selamat, R. Mashinchi, and K. Kuca, Determining of blood artefacts in endoscopic images using a software analysis, in *Computational Collective Intelligence*. vol. 9330.

[7] C.S.M. Cheng, Y.F. Lee, Ong, C. Yap, Z.L. Tsai, A. Mohla, M.E. Nongpiur, T. Aung, S.A. Perera, Inter-eye comparison of retinal oximetry and vessel caliber between eyes with asymmetrical glaucoma severity in different glaucoma subtypes (2016) *Clinical Ophthalmology*, 10, pp. 1315-1321.

[8] A. Dziubek, G. Guidobon, A. Harris, A.N. Hirani, E. Rusjan, W. Thistleton, Effect of ocular shape and vascular geometry on retinal hemodynamics: a computational model (2016) *Biomechanics and Modeling in Mechanobiology*, 15 (4), pp. 893-907.

[9] S. Zhang, L. She, X. Ge, Enhancement algorithms of retinal blood vessels based on curvelet conversion (2016) *Dongbei Daxue Xuebao/Journal of Northeastern University*, 37 (7), pp. 922-926.

[10] J. Blahuta, T. Soukup, and P. Cermak, How to detect and analyze atherosclerotic plaques in B-MODE ultrasound images: a pilot study of reproducibility of computer analysis, in *Artificial Intelligence: Methodology, Systems, and Applications*, Aimsa 2016. vol. 9883, C. Dichev and G. Agre, Eds., ed, 2016, pp. 360-363.

[11] J. Blahuta, T. Soukup, M. Jelinkova, P. Bartova, P. Cermak, R. Herzig, et al., A new program for highly reproducible automatic evaluation of the substantia nigra from transcranial sonographic images, *Biomedical Papers-Olomouc*, vol. 158, pp. 621-627, 2014.

[12] I. Bryjová, J. Kubicek, H. Skutova, Comparison and classification of acoustic levels of MRI sequences (2016) *IFMBE Proceedings*, 57, pp. 768-772.

[13] J. Kubicek, M. Penhaker, I. Bryjova, M. Augustynek, Classification method for macular lesions using fuzzy thresholding method (2016) *IFMBE Proceedings*, 57, pp. 239-244.

[14] J. Kubicek, J. Timkovic, M. Augustynek, M. Penhaker, M. Pokrývková, Optical nerve disc segmentation using circual integro differencial operator (2016) *Lecture Notes in Electrical Engineering*, 362, pp. 387-396.

[15] J. Kubicek, M. Penhaker, Fuzzy algorithm for segmentation of images in extraction of objects from MRI, 2014 *International Conference on Advances in Computing, Communications and Informatics (ICACCI)*, pp. 1422-1427, 2014.

[16] J. Kubicek, M. Penhaker, I. Bryjova, M. Kodaj, Articular cartilage defect detection based on image segmentation with colour mapping (2014), *Lecture Notes in Computer Science (including subseries Lecture Notes in Artificial Intelligence and Lecture Notes in Bioinformatics)*, 8733, pp. 214-222.

[17] K. BahadarKhan, A.A. Khaliq, M.A. Shahid, morphological Hessian based approach for retinal blood vessels segmentation and denoising

using region based Otsu thresholding (2016) *PLoS ONE*, 11 (7), art. no. e0158996.

[18] N. Strisciuglio, G. Azzopardi, M. Vento, N. Petkov, Supervised vessel delineation in retinal fundus images with the automatic selection of B-COSFIRE filters (2016) *Machine Vision and Applications*, pp. 1-13.